LAWRENCE
LIVERMORE
NATIONAL
LABORATORY

LLNL-JRNL-607873

X-ray driven implosions at ignition relevant velocities on the National Ignition Facility

N. B. Meezan, A. J. MacKinnon, D. G. Hicks, E. L. Dewald, R. Tommasini, S. Le Pape, T. Doeppner, T. Ma, D. R. Farley, D. A. Kalantar, D. A. Callahan, C. A. Thomas, S. T. Prisbrey, O. S. Jones, J. L. Milovich, D. S. Clark, M. B. Schneider, A. S. Moore, K. Widmann, J. A. Koch, J. D. Salmonson, K. P. Opachich, L. R. Benedetti, S. F. Khan, A. G. MacPhee, S. M. Glenn, D. K. Bradley, E. G. Dzenitis, B. R. Nathan, J. J. Kroll, A. V. Hamza, S. N. Dixit, L. J. Atherton, O. L. Landen, W. W. Hsing, L. J. Suter, M. J. Edwards, B. J. MacGowan, E. I. Moses, R. E. Olson, J. L. Kline, G. A. Kyrala, J. D. Kilkenny, A. Nikroo, K. Moreno, D. E. Hoover

December 12, 2012

Physics of Plasmas

Disclaimer

X-ray driven implosions at ignition relevant velocities on the National Ignition Facility

N. B. Meezan,* A. J. MacKinnon, D. G. Hicks, E. L. Dewald, R. Tommasini, S. Le Pape, T. Döppner, T. Ma, D. R. Farley, D. A. Kalantar, D. A. Callahan, C. A. Thomas, S. T. Prisbrey, O. S. Jones, J. L. Milovich, D. S. Clark, M. B. Schneider, A. S. Moore, K. Widmann, J. A. Koch, J. D. Salmonson, K. P. Opachich, L. R. Benedetti, S. F. Khan, A. G. MacPhee, S. M. Glenn, D. K. Bradley, E. G. Dzenitis, B. R. Nathan, J. J. Kroll, A. V. Hamza, S. N. Dixit, L. J. Atherton, O. L. Landen, W. W. Hsing, L. J. Suter, M. J. Edwards, B. J. MacGowan, and E. I. Moses

Lawrence Livermore National Laboratory,

P.O. Box 808, Livermore, CA 94551-0808

R. E. Olson

Sandia National Laboratory, Albuquerque, NM 87185

J. L. Kline and G. A. Kyrala

Los Alamos National Laboratory, Los Alamos, NM 87545

J. D. Kilkenny, A. Nikroo, K. Moreno, and D. E. Hoover

General Atomics, P.O. Box 85608, San Diego, CA 93286-5608

Abstract

Backlit convergent ablator experiments on the National Ignition Facility (NIF) [E. I. Moses *et al.* , Phys. Plasmas **16**, 041006 (2009)] are indirect drive implosions that study the inflight dynamics of an imploding capsule. Side-on, backlit radiography provides data used by the National Ignition Campaign to measure time-dependent properties of the capsule ablator including its center of mass radius, velocity, unablated mass, shell thickness, and peak density. Previously, Callahan [D. A. Callahan *et al.*, Phys. Plasmas **19**, 056305 (2012)] and Hicks reported backlit convergent ablator experiments demonstrating velocities approaching those required for ignition. Here, we present more recent results that appear to have demonstrated the NIF ignition velocity goal.

PACS numbers: 52.57Fg,28.52Cx,52.57Bc

* meezan1@llnl.gov

I. INTRODUCTION

In the inertial confinement fusion (ICF) hot-spot ignition scheme, kinetic energy from an imploding spherical pusher is converted upon stagnation to internal energy in the fusion fuel hot spot [1]. At the National Ignition Facility (NIF)[2], this is achieved via the indirect-drive method. The fusion capsule consists of a spherical shell of cryogenic deuterium-tritium (DT) fuel surrounded by a plastic (CH) ablator. Laser power deposited inside a gold or uranium hohlraum is converted to soft x-rays that impinge on the ablator. The ablator material absorbs the x-rays and explodes outward, accelerating the shell and fuel layer inward. In order to achieve a sufficiently high hot spot temperature to initiate thermonuclear burn, the maximum velocity of the cryogenic DT fuel pusher must reach $V_{fuel} \gtrsim 350$ km/s [3]. By the end of the acceleration phase, most (≈ 90 %) of the ablator material surrounding the cryogenic fuel layer has been removed.

Theoretically, to provide the most efficient acceleration, nearly all the ablator material should be removed from the capsule during acceleration—the ablation pressure then acts upon the minimum payload mass[4]. Only a very thin ablator layer is needed to protect the fuel from direct x-ray heating at the end of the implosion. Unfortunately, during the implosion's acceleration phase, the ablation front of the imploding shell is unstable to the Rayleigh-Taylor instability. Although the instability is partially stabilized by the ablation process, it is possible for defects on the capsule surface to grow to several hundred times their original size. It is therefore desirable to keep additional mass between the fuel layer and the ablation front to separate the hotspot from Rayleigh-Taylor growth at the ablation front. On the other hand, increasing the ablator mass of the capsule increases the laser energy and power needed to drive the fuel pusher to the required velocity.

For the baseline NIF ignition capsule design, these two competing design considerations of velocity and remaining ablator mass were balanced using radiation-hydrodynamics simulations. The resultant goal for the capsule is to achieve a fuel velocity $V_{fuel} = 370$ km/s with $M \geq 0.25$ mg of ablator mass remaining at the time of peak velocity[3]. Thus, one of the primary thrusts of the NIF ignition tuning campaign[5] has been to demonstrate that the laser/target system can achieve this goal. This paper describes recent experiments and supporting analysis suggesting that this goal has been nearly met ($V_{fuel} \geq 350$ km/s) with a 215 µm-thick silicon-doped CH capsule driven inside a uranium-walled hohlraum by a 520

TW, 1.86 MJ laser pulse.

We begin by describing how the fuel velocity and ablator mass of a DT-layered ignition capsule can be inferred from measurements of equivalent gas-filled symmetry capsules using the backlit convergent ablator experimental platform[6]. We briefly describe this platform and the supporting radiation-hydrodynamics simulations with the code HYDRA[7] that are used to interpret the data. We then compare simulations and data in the "rocket curve" (V vs. M) plane, motivated by a rocket acceleration model of the shell [4]. While both simulations and data lie along a nearly-universal rocket curve, the data suggest the capsules reach a given velocity with less ablator mass remaining than predicted by HYDRA simulations. This finding motivated experiments with a 20 µm-thicker capsule, to ensure $M \geq 0.25$ mg at $V_{fuel} = 370$. We then describe a symmetry-capsule experiment using this thicker capsule driven by a 520 TW, 1.86 MJ laser pulse, near the edge of NIF's current operating capability. X-ray drive and implosion timing data from this experiment, together with velocity measurements from companion convergent-ablator experiments and scaling calculations in HYDRA, suggest that this symmetry capsule experiment achieved an implosion trajectory equivalent to the ignition (M, V) goal.

II. EXPERIMENTAL SETUP

Here, we briefly review the backlit convergent ablator experiments, including descriptions of the targets, analysis methods, and supporting simulations. A comprehensive description of the NIF convergent ablator experiments can be found in the recent paper by Hicks *et al.*[8]. The convergent ablator platform uses a nearly monochromatic x-ray backlighter at 8.95 keV (Zn) or 10.3 keV (Ge) to generate time-dependent absorption radiographs of the imploding ablator. Two of the 48 laser quads on NIF are diverted from the hohlraum to a thin (5–15 µm) foil mounted outside of the hohlraum to generate an area backlighter. X-rays from the backlighter travel through two window slots on opposite sides of the hohlraum and the imploding capsule in the middle. Two limbs on the capsule equator (perpendicular to the hohlraum axis) are imaged by slit onto a gated x-ray camera (GXD) or an x-ray streak camera (DISC). Generally, a gas-filled symmetry capsule or"symcap" is imploded; however, the technique also works for capsules with a cryogenic fuel layer. At these backlighter energies, the hydrogen fuel layer is transparent and the technique only radiographs the

ablator material.

The resulting backlit-radiographs are inverted, assuming spherical symmetry, to generate a radial profile of the absorption coefficient $\kappa\rho\,(r)$, where κ is the opacity of the ablator at the photon energy of the backlighter and ρ is the ablator density. The density profile $\rho\,(r)$ is found by dividing $\kappa\rho$ by the ablator opacity profile $\kappa\,(r)$. The data inversion process is very challenging—the analysis must reject hard x-ray background, account for the resolution of the detector system, and simultaneously fit both the unknown backlighter profile and density profile. Challenges associated with the inversion process are described in more detail in [6, 9].

In practice, since the density profile $\rho\,(r)$ is not measured with sufficient spatial resolution to directly compare with radiation-hydrodynamics simulations, integral moments of the density are used to evaluate the implosion performance. In this paper, we focus on the center-of-mass position of the ablator, the center-of-mass velocity of the ablator (obtained by taking the time derivative of the radius), and the mass of the ablator. The ablator mass is

$$M = \int \rho\,(r)\, r^2 \mathrm{d}r, \tag{1}$$

the center-of-mass radius is defined as

$$R_{CoM} = \frac{\int r\rho\,(r)\, r^2 \mathrm{d}r}{\int \rho\,(r)\, r^2 \mathrm{d}r}, \tag{2}$$

and the velocity of the ablator center-of-mass is simply

$$V_{CoM} = \frac{\mathrm{d}R_{CoM}}{\mathrm{d}t}. \tag{3}$$

The limits of integration in Eqs. 1 and 2 are taken as the inner surface of the ablator and the ablation front. For HYDRA simulations, the ablation front is defined as the radius at which the local T_{RAD}^4 drops to 10 % of the incident x-ray flux. For the data, it might be possible to identify the radius of the ablation front directly from the radiographs (see [9]) and incorporate this knowledge into the analysis. In practice, the data analysis assumes that the ablated material has negligible opacity—the outside edge of the inverted $\rho\,(r)$ is *de facto* the ablation front. This is a good approximation for undoped CH plastic; however, for the silicon-doped layers of the capsules described in this paper, the opacity of the hot, ablated blow-off at the backlighter photon energy $h\nu = 8.95$ keV can be appreciable, greater than 50 % of the cold opacity. The fact that the location of the ablation front is not obvious in the inverted $\rho\,(r)$ introduces an inconsistency when comparing to simulations. Efforts

to develop metrics that allow direct comparison of experimental and simulated radiographs without an inversion step in the analysis are ongoing[9].

A. Targets

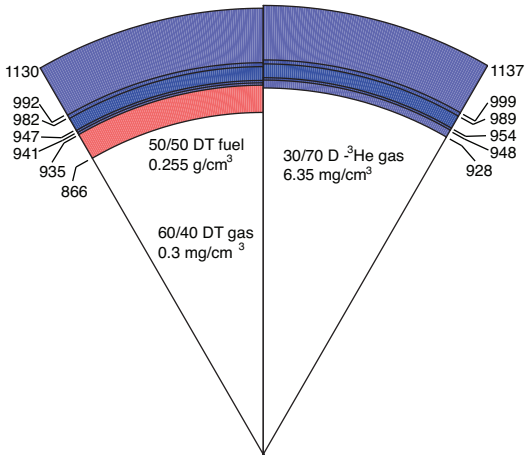

FIG. 1. Capsule pie diagrams for the nominal "Rev 5" ignition capsule (left) and symmetry capsule (right) with silicon dopant layers. Dimensions are in microns. Both capsules use the same podium profile for the Si dopant, with clean CH (plastic) on the inner-most and outer-most layers. The central layers have nominally 1 %, 2 %, and 1% silicon (by atom) doped in the plastic.

Capsule pie diagrams for the nominal "Rev 5" ignition capsule (left) and symmetry capsule (right) with silicon dopant layers are show in Fig. 1. The symmetry capsule or symcap replaces the cryogenic fuel layer on the inside of the capsule with an equivalent mass of CH. The central gas in the cryogenic layered target is the residual vapor pressure from the fuel ice at the layering temperature. The symcap is filled with gas to provide x-rays and fusion neutrons for diagnostic purposes. Both capsules use a multi-step profile for the Si dopant, with clean CH (plastic) on the inner-most and outer-most layers. The central layers have nominally 1 %, 2 %, and 1% silicon (by atom) doped in the plastic. This design differs slightly from the previous capsule design with germanium dopants[3]. The silicon capsules are 5 µm thicker—195 µm and 209 µm for the ignition capsule and symcap, respectively. Another variation on the capsule is the use of more silicon dopant. The "2×" Si design

is nominally the same as the nominal "1×" Si design describe above, but the amount of silicon in the dopant podium is doubled to 2 %, 4 %, and 2% silicon by atom.We have also used thicker capsules 215 µm and 229 µm for the DT and symcap, respectively. The other dimensions are nominally the same for these thicker capsules. Differences in capsule inner diameter can result from the choice of particular mandrels for the CH coating process and also depend on the pyrolysis process for mandrel removal.

The hohlraums for the experiments described here were 5.75 mm in diameter and 9.43 mm long, with 3.1 mm or 3.373 mm diameter laser-entrance holes (LEHs), as described by Callahan etal [10]. A mixture of gold-walled and uranium-walled hohlraums were used for the experiments. A variety of laser pulses drove the experiments, with powers ranging from 330 TW to 420 TW and energies from 1.2 MJ to 1.9 MJ. More details on the experimental targets and laser pulses can be found in the paper by Hicks *et al.*[8].

B. Hydrodynamics simulations

HYDRA is a 3D multi-physics radiation-hydrodynamics code that attempts to include all of the physics needed to model ICF experiments [7].Two kinds of calculations are described in this paper. The 2D integrated (hohlraum + capsule) post-shot simulations described here use the "high-flux model"—electron thermal conduction with a flux-limiter $f = 0.15$ and the DCA non-LTE atomic physics model—developed after the NIF hohlraum energetics campaign of 2009 [11]. The input laser sources are adjusted to account for backscattered light and for cross-beam transfer occurring in the hohlraum plasma [12–14]. In addition, the laser source is further degraded to match experimental shock-front and ablator data, as described by Jones *et al.*[15].

Capsule-only 1D HYDRA simulations are also used to translate the V_{CoM} measured in a convergent ablator experiment to the equivalent fuel velocity V_{fuel} of a DT capsule driven by an equivalent x-ray source. Since a symcap has the same mass as its equivalent DT capsule, their acceleration histories are equivalent. However, the velocity of the fuel in a DT capsule begins to diverge from the velocity of the ablator at small radius due to convergence effects—the DT fuel is squeezed towards the center due to spherical convergence. Simulations show that the local velocity of the ablator or fuel at a given time increases towards the center of the shell (c.f. Fig. 4 of [10]). The maximum of V_{fuel} in a DT capsule is typically 10–15

% higher than that of V_{CoM} for the equivalent symcap. Note that V_{fuel} is defined as the mass-average velocity of the cryogenic fuel layer.

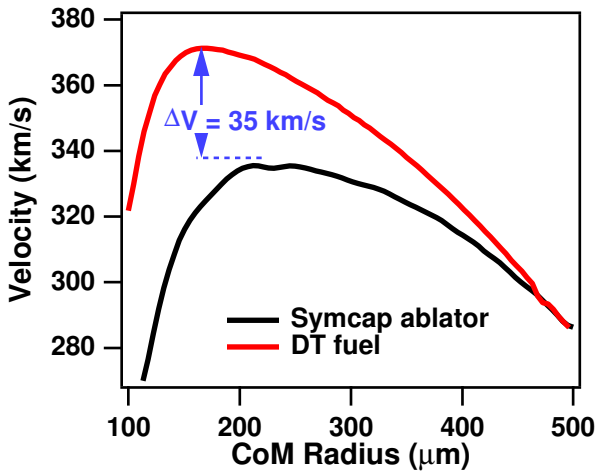

FIG. 2. Velocity vs. ablator center-of-mass radius R_{CoM} for two 1D HYDRA calculations using the same x-ray drive source. The black curve shows the center-of-mass velocity $V_{CoM} = \frac{d}{dt}R_{CoM}$ for a symmetry capsule—this quantity is measured in backlit convergent ablator experiments. The red curve shows the mass-average fuel velocity V_{fuel} for the equivalent DT-layered ignition capsule. The fuel velocity is higher than the ablator velocity due to convergence effects at small radius. The maximum of V_{fuel} is typically 10–15 % higher than that of V_{CoM}.

Capsule-only 1D HYDRA simulations are also used to aid in translating measured x-ray bang-times (the times of peak x-ray emission from the capsule) from symmetry experiments (which lack direct measurements by backlit radiography) to ablator center-of-mass velocities. We start with a frequency-dependent-source or FDS (spectral intensity as a function of time and photon energy $h\nu$) generated from a hohlraum simulation using the methodology described above. The source is further "tuned" in the foot (pulses 1-3) to match available shock-timing data, using the methods described by Clark *et al.*[16]. The peak flux of the source is then scaled as appropriate to assist with data interpretation. Timing data for the main shock were not measured for this pulse/capsule combination and are not used.

III. ROCKET CURVES

The convergent ablator platform measures the implosion trajectory and mass over many times, allowing the velocity and mass to be plotted vs. time or radius for comparison to HYDRA simulations; however, it is particularly insightful to compare the two in the "rocket curve" plane, velocity vs. mass. This is because the acceleration of the ablator and fuel of an ICF capsule are well-described by a generalized rocket model, described in detail by Saillard [4]. At the time of the main shock breakout (the beginning of the capsule acceleration phase), the rocket model simplifies to three ordinary differential equations,

$$\begin{aligned} \frac{\mathrm{d}R}{\mathrm{d}t} &= U, \\ \frac{\mathrm{d}M}{\mathrm{d}t} &= -4\pi R^2 \dot{m}_a, \\ M\frac{\mathrm{d}U}{\mathrm{d}t} &= -4\pi R^2 p_a. \end{aligned} \tag{4}$$

Here, U is the mass-average velocity of the shell, R is the ablation-front radius, and M is the mass of the shell. The mass-ablation rate $\dot{m}_a$ and ablation pressure p_a are functions of the applied radiation flux on the capsule. The power of this model is that it describes the time-histories of R, U, and M without considering the waves, shocks, and rarefactions moving through the shell [4].

This system can be approximately solved, recovering the well-known rocket equation,

$$U \simeq \frac{p_a}{\dot{m}_a} \ln\left(\frac{M}{M_0}\right) \tag{5}$$

The quantity $v_{ex} = \frac{p_a}{\dot{m}_a}$, sometimes called the "exhaust velocity," [5] is a slow function of the radiation temperature, $v_{ex} \propto T_R^{\frac{1}{2}}$. Thus, the shell velocity at any point in the capsule trajectory up to the end of the acceleration phase can be related to the fraction of mass ablated from the shell.

A. Ignition goal rocket curves

Rocket curves for a DT capsule that meets the ignition (M, V_{fuel}) goal and its corresponding symcap are compared in Fig. 3. These rocket curves were generated from the same two 1D HYDRA calculations shown in Fig. 2. The rocket model approximation Eq. 5 agrees well with the HYDRA simulation for $v_{ex} = 167$ km/s. This is slightly higher than the sound

speed $c \approx \sqrt{ZT_R/M_i} = 125$ km/s at $T_R = 300$ eV (using Z=3.5 for CH). The formulas for v_{ex} in Saillard[4] (derived from fits to radiation-hydrodynamics simulations) give 167 km/s for $T_R = 265$ eV or $v_{ex} = 178$ km/s for $T_R = 300$ eV.

For this drive, the unablated mass for the DT capsule when it reaches $V_{fuel} = 370$ km/s is $M = 0.27$ mg, slightly higher than the ignition goal $M = 0.25$ mg. The velocity difference between the symcap and DT capsules described in Fig. 2, $\Delta V = 35$ km/s, is evident, as well as a difference in final ablator mass of $\Delta M = 0.21$ mg. This is slightly larger than the nominal fuel mass of 0.17 mg. These two numbers $(\Delta V, \Delta M)$ allow us to define the equivalent mass/velocity goal for a *symcap*, $V_{CoM} = 335$ km/s, $M = 0.46$ mg.

The key physical insight provided by the rocket model Eq. 4 is that for a given capsule, due to the slow dependence of v_{ex} on T_R, changing the intensity or duration of the main drive will simply move the final (U, M) of the capsule further up or down the rocket curve. Together with the symcap mass/velocity goal, defined above, this insight simplifies the NIF velocity tuning campaign to two requirements:

1. Determine the initial capsule mass required to pass through the symcap velocity goal $V_{CoM} = 335$ km/s with ablator mass remaining $M \geq 0.46$ mg

2. Determine the laser power and energy needed to drive this capsule to the velocity goal

B. Experimental rocket curves for 209 μm capsules

As mentioned above, the key insight provided by the rocket model changing the main drive on a capsule simply moves the final (U, M) further up or down the rocket curve. The large database of convergent ablator data on NIF provides a test of this insight, as this database contains many shots with basically the same capsule but different drive histories. Fig. 4 compares the velocity, mass data (V_{CoM}, M) from twelve convergent ablator experiments to their corresponding 2D post-shot HYDRA calculations. Each point in Fig. 4 represents one data point from an experiment. For the four-strip gated detector, each V_{CoM} point is obtained by finite differencing R_{CoM} on adjacent strips, whereas M is interpolated between strips. A similar technique is used for the DISC streak camera, using a group of adjacent pixels (in time) in place of a strip. Note that the center-of-mass velocity V_{CoM} is not identical to the mass-average velocity U from Eq. 4, although they show similar qualitative

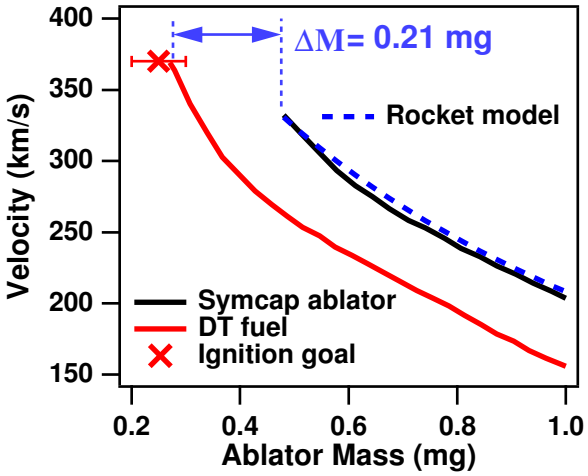

FIG. 3. Rocket curves for a thicker (215 µm) DT capsule and (229 µm) symcap from two 1D HYDRA calculations that use the same x-ray drive source. The blue dashed curve is simply Eq. 5, $U = -167 \ln\left(\frac{M}{M_0}\right)$, and passes through the HYDRA symcap simulation. The ignition mass/velocity goal $V_{fuel} = 370$ km/s, $M = 0.25$ mg is shown as a red ×. The error bars $\Delta M = \pm 0.05$ mg represent the total uncertainty in inferring the mass from a convergent ablator experiment.

behavior. Both quantities can be readily extracted from HYDRA simulations and compared. The center-of-mass velocity V_{CoM} is systematically larger than the mass-weighted velocity U by 5–15 km/s, comparable to the error bars on typical V_{CoM} data. Early in the implosion, the relative difference between V_{CoM} and U can be as high as 10 % but drops to 2 % at peak velocity.

All of the experiments in Fig. 4 were performed on nominal-thickness (209 µm ± 3 µm) symcaps. Ten of the twelve capsules were 1× Si-doped; the other two were 2× Si-doped. A mixture of gold-walled and uranium-walled hohlraums were used for the experiments, with 3.1 mm or 3.373 mm diameter laser-entrance holes (LEHs). A variety of laser pulses drove the experiments, with powers ranging from 330 TW to 420 TW and energies from 1.2 MJ to 1.9 MJ. The detailed configuration for each experiment can be found in the paper by Hicks *et al.*[8].

The data generally lie on the simulated rocket curves within the measurement uncertainty. The width of the bundle of simulated rocket curves is $\delta M \approx 0.2$ mg in mass at a given velocity or $\delta V_{CoM} \approx 25$ km/s in velocity at a given mass. This width is fairly small, comparable to the measurement uncertainties (the error bars in Fig. 4). The source of this width (δV_{CoM})

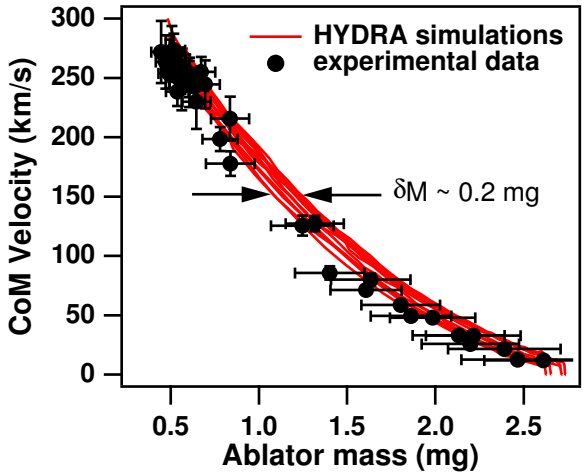

FIG. 4. Rocket curves for nominal (209 µm ± 3 µm) symcaps from twelve convergent ablator experiments and their corresponding 2D post-shot HYDRA calculations. The twelve shots vary in laser peak power, capsule dopant concentration, LEH size, and hohlraum wall material. The data generally lie on the simulated rocket curves within the measurement uncertainty. The thickness of the bundle of simulated rocket curves is $\delta M \approx 0.2$ mg in mass and $\delta V_{CoM} \approx 25$ km/s in velocity.

at a given mass is not completely understood—it is likely due to changes in the x-ray drive spectrum incident on the capsule.

Zooming in on the rocket curves (Fig. 5), we see that many of the data points lie below the simulated curves, i.e., for a given velocity, the amount of ablator mass remaining is smaller than in simulations; however, for most of the data, the distance from the simulation cluster is comparable to the experimental uncertainty. Several efforts are under way to reduce the uncertainty in the remaining mass measurement. Backlighter-only shots provide more detailed knowledge of the backlighter profile, potentially reducing the uncertainty inherent in the simultaneous density-profile/backlighter-profile fit. Higher magnification experiments focusing on a single capsule limb rather than the standard two-limb technique provide a flatter backlighter-profile, further reducing this uncertainty. In addition, better understanding of the absolute hard x-ray background from the hohlraum, the opacity of the ablator, and the spectral purity of the backlighter are needed to reduce the uncertainty of the mass measurement.

The dashed line in Fig. 5 shows an additional HYDRA simulation of a nominal 1× Si capsule that reaches the symcap V_{CoM} goal. This rocket curve lies to the high-mass side

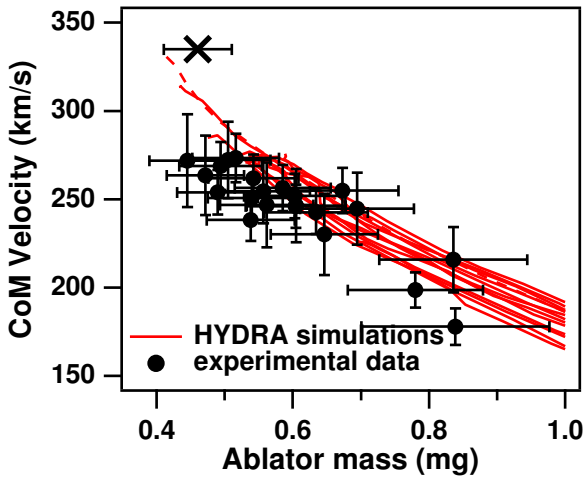

FIG. 5. Rocket curves for nominal (209 µm ± 3 µm) symcaps from twelve convergent ablator experiments and their corresponding 2D post-shot HYDRA calculations, focused near the end of the acceleration phase. The symcap mass/velocity goal, $V_{CoM} = 335$ km/s, $M = 0.46$ mg, is shown by the black ×. A HYDRA simulation of the nominal 1× Si capsule that reaches the symcap velocity goal is shown by the red dashed line. This rocket curve reaches $V_{CoM} = 335$ km/s with mass ≈ 0.05 mg below the goal of $M = 0.46$ mg.

of the data cluster but passes the ignition velocity goal with 0.05 mg less mass than the ignition symcap goal of 0.46 mg. This suggests that a thicker capsule with higher initial mass is needed to reach the (M, V) goal.

C. Experimental rocket curves for 20 µm thicker capsules

Results from a convergent ablator experiment with a 20 µm thicker (≈ 229 µm) capsule (NIF shot N120418) are show in blue in Fig. 6. These results are compared to convergent ablator experiments with the nominal thickness capsule driven by a 330 TW, 1.6 MJ laser pulse (a subset of the twelve experiments shown in Figs. 4 and 5). The thicker capsule experiment, designed to drive the capsule to the same peak velocity $V_{CoM} = 280$ km/s, required a laser pulse with 385 TW and 1.9 MJ. The thicker capsule starts with ≈ 0.4 mg more mass than the nominal capsule but reaches peak velocity with ≈ 0.1 mg more unablated mass. The blue dashed line shows a HYDRA simulation of the same capsule that reaches the velocity goal $V_{CoM} = 335$ km/s. This simulation achieves the goal with slightly more mass

than the goal $M = 0.46$ mg. Thus, the data from the convergent ablator experiment with a 20 µm thicker ablator are consistent with a rocket curve that passes through the ignition (M, V) goal; however, driving this target to the velocity goal will require substantially higher laser power than 385 TW.

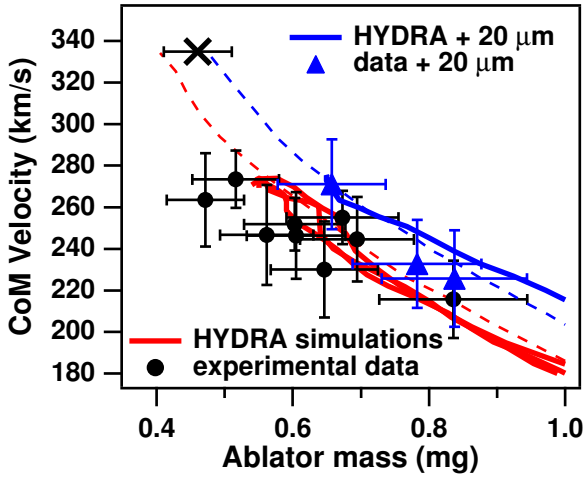

FIG. 6. Rocket curves for nominal (209 µm ± 3 µm) and thick (≈ 229 µm) symcaps from ?? convergent ablator experiments designed to reach $V_{CoM} = 280$ km/s and their corresponding 2D post-shot HYDRA calculations. The red curves and black data points are a subset of the twelve experiments shown in Fig. 5. The red dashed line is as in 5. The blue data points and solid curve are results for a backlit experiment with a 20 µm thicker (≈ 229 µm) capsule. The blue dashed curve is a simulation of this thicker capsule driven to the symcap velocity goal, $V_{CoM} = 335$ km/s.

IV. 520 TW SYMCAP EXPERIMENT

The NIF facility recently performed a full laser-system shot to demonstrate total laser power $P > 500$ TW and total energy $E > 1.8$ MJ. The target for this shot was a thick 231 µm, 2× Si symcap in a uranium-walled hohlraum. The results of this important experiment, N120705, are described in more detail by Kline *et al.*[17]. This experiment did not use backlit radiograph to directly measure V_{CoM}, as this level of laser power and energy cannot be delivered to the hohlraum while directing two of NIF's 48 quads to a backlighter foil. However, we can use the V_{CoM} data from a similar but lower-power convergent ablator experiment N121007, along with x-ray drive and bang-time data, to infer V_{CoM} for N120705.

Below, we argue that N120705 achieved symcap goal, $V_{CoM} = 335$ km/s, $M = 0.46$ mg, with a 520 TW, 1.86 MJ laser pulse.

A. Simulation drive source

Capsule-only 1D HYDRA simulations are used to translate the measured the time of peak capsule x-ray emission ("x-ray bang-time"') for N120705 to the ablator center-of-mass velocity. We start with a tuned FDS as described in section II B. In order to infer the implosion velocity from the bang-time, it is important to use a drive history with the correct start time and rate-of-rise for the main drive, as these determine the launch time and strength of the main shock. For example, if the main shock in the simulation is launched late, resulting in late acceleration of the ablator, the velocity V_{CoM} inferred by matching the bang-time will be too high. Therefore, we use a drive source derived directly from the data rather than a frequency-dependent-source extracted from a HYDRA hohlruam simulation. Hohlraum simulations are used to set the spectral content of the FDS, but not the shape or level of the main drive. For the main pulse, we construct the source intensity such that the T_{RAD} vs. time qualitatively matches the experimental $T_{RAD}\,(t)$ inferred from DANTE and SXI data. The method for constructing this source is described in [18] and is repeated in brief below.

The brightness temperature of the hohlraum is calculated from the measured radiant intensity Φ [GW/sr] of the hohlraum LEH and the effective source-size A_{LEH},

$$T_{RAD} = \left(\frac{\pi I_{av}}{\sigma}\right)^{1/4} = \left(\frac{\pi \Phi}{\sigma A_{LEH} \cos\theta}\right)^{1/4}. \tag{6}$$

Here, I_{av} is the total average x-ray intensity [GW/sr/cm^2] and σ is the Stefan-Boltzmann constant. The radiant intensity Φ is measured by the DANTE diagnostic, an 18 channel array of filtered x-ray diodes, at an angle $\theta = 37.5°$ [19, 20].

The source-size A_{LEH} is found from the two static x-ray imagers (SXI's)[21], time-integrated x-ray pinhole cameras that view the LEH at $\theta = 18°$ and $\theta = 19°$. The high energy channel (3 keV $< h\nu <$ 5 keV) image delineates the dense, absorbing part of the LEH from the "clear area," where x-rays leaving the hohlraum are not significantly attenuated before reaching the DANTE. This image identifies A_{LEH} in Eq. 6. Only x-rays from the clear area should be counted in I_{av} for calculating T_{RAD}. The monochromatic channel ($h\nu \approx 870$ eV, near the peak of the blackbody spectrum for $T = 300$ eV) shows x-rays that

originate from within the clear aperture as well as a "halo" of x-rays either emitted from or attenuated by the gold LEH plasma. This image identifies the "halo correction" factor f, the fraction of x-rays outside the clear area.

We approximate the time-dependent clear area A_{LEH} and halo-factor f as varying linearly between their initial values at $t = 0$ and the SXI data at the time of peak intensity, $t = t_{peak}$,

$$A_{LEH}(t) = \pi R_{LEH}^2 \left(1 - \frac{t}{t_{peak}}\right) + A_{LEH,SXI} \left(\frac{t}{t_{peak}}\right)$$
$$f(t) = f_{SXI} \left(\frac{t}{t_{peak}}\right)$$

After correcting the flux seen by the capsule for the area subtended by the LEH's, we come to the final expression for $T_{RAD}(t)$,

$$T_{RAD}(t) = \left(\frac{\pi [1 - f(t)] \Phi(t)}{\sigma A_{LEH}(t) \cos\theta} \frac{L}{\sqrt{R_{LEH}^2(t) + L^2}}\right)^{1/4}. \quad (7)$$

Here, L is the hohlraum half-length and the time-dependent LEH radius $R_{LEH}(t) = \sqrt{A_{LEH}(t)/\pi}$.

B. Velocity measurement and inference

The overall intensity of the main drive is then scaled in a series of 1D HYDRA simulations (using the as-shot capsule dimensions and properties) to generate a lookup-curve of peak ablator velocity V_{CoM} vs. time of peak capsule x-ray emission. The $T_{RAD}(t)$ for the FDS that matches the measured bang-time of the 520 TW symcap shot N120705 is compared with the data-inferred $T_{RAD}(t)$ in Fig. 7. The same FDS sources are also applied to an ideal thickness (215 µm) 2 × Si DT ignition capsule to generate a lookup-curve of fuel velocity V_{fuel} vs. x-ray bang-time. Thus, for the measured experimental x-ray bang-time, we can infer the symcap ablator velocity V_{CoM} and the equivalent DT fuel velocity V_{fuel}. The look-up curve V_{CoM} vs. x-ray bang-time for symcap shot N120705 and the corresponding V_{fuel} vs. x-ray bang-time are shown in Fig. 8.

Note that the drive resulting from this procedure is not unique because the current data analysis does not highly constrain the spectral content of the drive—a given $T_{RAD}(t)$ drives the capsule differently depending on the spectral content of the drive. As the spectral hardness is varied within reasonable bounds, the peak T_{RAD} needed to drive the HYDRA

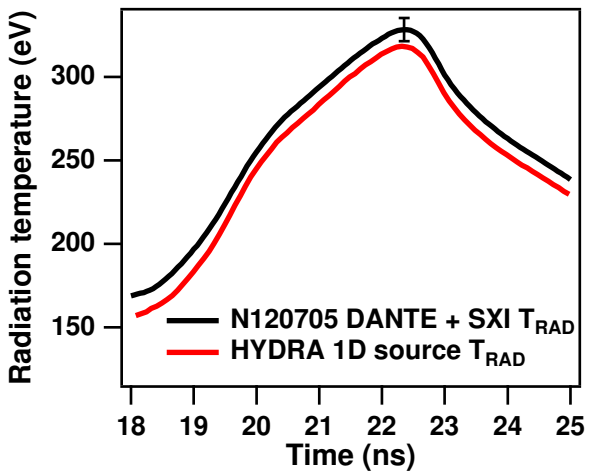

FIG. 7. Radiation brightness temperature T_{RAD} inferred from the DANTE and SXI diagnostics (cf. Eq. 7) for the 520 TW symcap shot N120705. The T_{RAD} for the frequency-dependent-source (FDS) used in the 1D HYDRA flux-scaling is shown in red for comparison. The launch time, rate-of-rise, and general shape of the FDS T_{RAD} are taken from the experimental data. The 1D HYDRA simulation using this source reproduces the measured x-ray bang-time of N120705. The maximum T_R of this source is slightly lower than the data using an error bar $\delta T_R \approx \pm 7$ eV to represent the combined uncertainty of DANTE, SXI, and the analysis method approximations

simulation to the measured x-ray bang-time can vary by more than 10 %; however, the variation in the look-up curve V_{CoM} vs. x-ray bang-time is much smaller than this.

Velocity data from a backlit convergent ablator experiment with the same laser pulse but slightly-reduced power and energy (N121007) are used to validate the 1D HYDRA lookup-curve. The laser pulses for the 520 TW symcap N120705 and the corresponding convergent ablator shot N121007 are shown in Fig. 9. The power delivered to the hohlraum for convergent ablator shot N121007 was reduced from 520 TW to 470 TW due to using two NIF quads for the backlighter. A third quad was dropped from the shot due to a mechanical failure. The reduced power and energy of the laser pulse resulted in a measured x-ray bang-time of 23.8 ns $\pm$0.1 ns, 400 ps later than the 24.2 ns $\pm$0.1 ns measured for the 520 TW symcap N120705. This Δt is slightly longer than predicted by HYDRA hohlraum simulations. The maximum ablator velocity measured on N121007—V_{CoM} = 295 km/s—lies just above the 1D HYDRA lookup-curve. This data point "pins the curve," suggesting that the timing, rate-of-rise, and shape of the 1D drive source are a suitably accurate representation of the

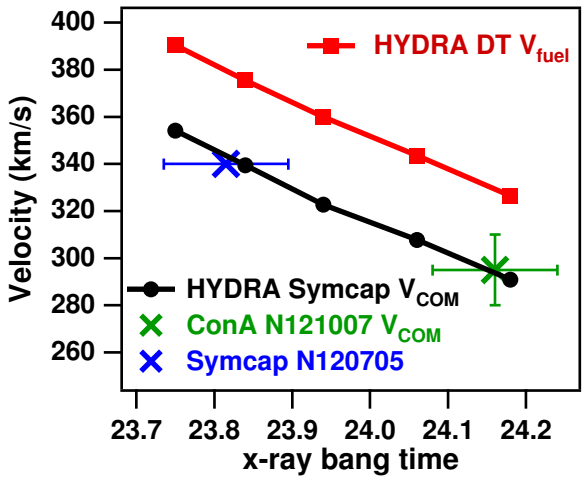

FIG. 8. Velocity vs. x-ray bang-time for symmetry capsule shot N120705 and convergent ablator shot N121007, compared with a 1D HYDRA flux-scaling. The convergent ablator data for center-of-mass velocity (V_{CoM}) and x-ray bang-time "pin" the scaling, allowing a velocity estimate for the higher-power N120705 shot based only on its bang-time.

actual drive on the capsule in the experiment.

The measured x-ray bang time $t = 23.8$ ns ± 0.1 ns for N120705 lies at $V_{CoM} \approx 340$ km/s on the HYDRA lookup-curve in Fig. 8, slightly exceeding the campaign goal. This corresponds to a fuel velocity $V_{fuel} = 375$ km/s for an 215 µm-thick ignition capsule driven by the same x-ray source. Previous data (Fig. 6) show that this capsule's rocket curve passes through the velocity goal with ablator mass-remaining slightly above the mass goal. Therefore, this experiment appears to have met the symcap (M, V) goal, $M \geq 0.45$ mg at $V_{fuel} = 335$ km/s—equivalent to meeting the ignition (M, V) goal, $M \geq 0.25$ mg at $V_{fuel} = 370$ km/s (cf. Fig 3). The uncertainty in bang-time $\delta t = 100$ ps, combined with the uncertainty in velocity for the backlit radiography data, $\delta V = 15$ km/s, combine to give an overall uncertainty of $\delta V \approx 25$ km/s in this inference. Thus, we can say with high confidence that the experiment N120705 demonstrated the equivalent of $V_{fuel} \geq 350$ km/s.

V. CONCLUSION

The convergent ablator platform allows fuel velocity and ablator mass of a DT-layered ignition capsule to be inferred from backlit-radiography measurements of an equivalent gas-

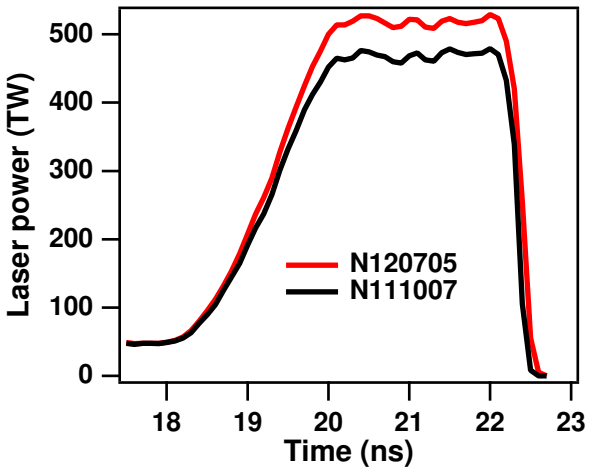

FIG. 9. Laser power delivered to the hohlraum for the symcap shot N120705 and the corresponding convergent ablator shot N121007. The average peak-power was 520 TW for N120705 and 470 TW for N121007. The requested power for N121007 was reduced from 514 TW to 500 TW. The power was further reduced due to diverting two quads to the backlighter foil and losing a third quad to mechanical failure. These laser pulses correspond to the $\times$ symbols in Fig. 8

filled symmetry capsule. Comparing the supporting radiation-hydrodynamics simulations with the code HYDRA to experimental data in the "rocket curve" V vs. M plane shows that the capsules generally move along nearly universal rocket-curves, as predicted by the simple rocket acceleration model of the shell [4]; however, the data tend to show lower ablator mass M than HYDRA simulations at a given velocity V. For the nominal ignition capsule thickness, these data and simulations extrapolate to reaching the ignition velocity goal $V_{fuel} = 370$ km/s with ablator mass below the goal $M = 0.25$ mg. This result motivated experiments with a 20 µm-thicker capsule, which extrapolate to $M \geq 0.25$ mg at $V_{fuel} = 370$ km/s. A symmetry-capsule experiment using this thicker capsule driven by a 520 TW, 1.86 MJ laser pulse, near the edge of NIF's current operating capability, appears to have achieved an implosion trajectory equivalent to the ignition (M, V) goal. The equivalent of $V_{fuel} \geq 350$ km/s has been demonstrated with high confidence. Remaining goals for the campaign include reducing the uncertainty in measuring ablator mass. The current uncertainty, $\delta M = 0.05$ mg, is comparable to the difference between nominal and +20 µm thick capsules.

ACKNOWLEDGMENTS

The author would like to acknowledge the efforts of the NIF operations, laser performance, target diagnostics, and target fabrication teams. This work was performed under the auspices of the U.S. Department of Energy by Lawrence Livermore National Laboratory under Contract DE-AC52-07NA27344.

---

[1] J. Lindl, P. Amendt, R. Berger, S. Glendinning, S. Glenzer, S. Haan, R. Kauffman, O. Landen, and L. Suter, Physics of Plasmas **11**, 339 (2004).

[2] E. Moses, R. Boyd, B. Remington, C. Keane, and R. Al-Ayat, Physics of Plasmas **16**, 041006 (13 pp.) (2009).

[3] S. W. Haan, J. D. Lindl, D. A. Callahan, D. S. Clark, J. D. Salmonson, B. A. Hammel, L. J. Atherton, R. C. Cook, M. J. Edwards, S. Glenzer, A. V. Hamza, S. P. Hatchett, M. C. Herrmann, D. E. Hinkel, D. D. Ho, H. Huang, O. S. Jones, J. Kline, G. Kyrala, O. L. Landen, B. J. MacGowan, M. M. Marinak, D. D. Meyerhofer, J. L. Milovich, K. A. Moreno, E. I. Moses, D. H. Munro, A. Nikroo, R. E. Olson, K. Peterson, S. M. Pollaine, J. E. Ralph, H. F. Robey, B. K. Spears, P. T. Springer, L. J. Suter, C. A. Thomas, R. P. Town, R. Vesey, S. V. Weber, H. L. Wilkens, and D. C. Wilson, Physics of Plasmas **18**, 051001 (2011).

[4] Y. Saillard, Nuclear Fusion **46**, 1017 (2006).

[5] O. L. Landen, J. Edwards, S. W. Haan, H. F. Robey, J. Milovich, B. K. Spears, S. V. Weber, D. S. Clark, J. D. Lindl, B. J. MacGowan, E. I. Moses, J. Atherton, P. A. Amendt, T. R. Boehly, D. K. Bradley, D. G. Braun, D. A. Callahan, P. M. Celliers, G. W. Collins, E. L. Dewald, L. Divol, J. A. Frenje, S. H. Glenzer, A. Hamza, B. A. Hammel, D. G. Hicks, N. Hoffman, N. Izumi, O. S. Jones, J. D. Kilkenny, R. K. Kirkwood, J. L. Kline, G. A. Kyrala, M. M. Marinak, N. Meezan, D. D. Meyerhofer, P. Michel, D. H. Munro, R. E. Olson, A. Nikroo, S. P. Regan, L. J. Suter, C. A. Thomas, and D. C. Wilson, Physics of Plasmas **18**, 051002 (2011).

[6] D. G. Hicks, B. K. Spears, D. G. Braun, R. E. Olson, C. M. Sorce, P. M. Celliers, G. W. Collins, and O. L. Landen, Physics of Plasmas **17**, 102703 (2010).

[7] M. M. Marinak, G. D. Kerbel, N. A. Gentile, O. Jones, D. Munro, S. Pollaine, T. R. Dittrich, and S. W. Haan, Physics of Plasmas **8**, 2275 (2001).

[8] D. G. Hicks, N. B. Meezan, E. L. Dewald, A. J. Mackinnon, R. E. Olson, D. A. Callahan, T. Doppner, L. R. Benedetti, D. K. Bradley, P. M. Celliers, D. S. Clark, P. D. Nicola, S. N. Dixit, E. G. Dzenitis, J. E. Eggert, D. R. Farley, J. A. Frenje, S. M. Glenn, S. H. Glenzer, A. V. Hamza, R. F. Heeter, J. P. Holder, N. Izumi, D. H. Kalantar, S. F. Khan, J. L. Kline, J. J. Kroll, G. A. Kyrala, T. Ma, A. G. MacPhee, J. M. McNaney, J. D. Moody, M. J. Moran, B. R. Nathan, A. Nikroo, Y. P. Opachich, R. D. Petrasso, R. R. Prasad, J. E. Ralph, H. F. Robey, H. G. Rinderknecht, J. R. Rygg, J. D. Salmonson, M. B. Schneider, N. Simanovskaia, B. K. Spears, R. Tommasini, K. Widmann, A. B. Zylstra, G. W. Collins, O. L. Landen, J. D. Kilkenny, W. W. Hsing, B. J. MacGowan, L. J. Atherton, and M. J. Edwards, Physics of Plasmas **19**, 122702 (2012).

[9] R. E. Olson, D. G. Hicks, N. B. Meezan, J. A. Koch, and O. L. Landen, Review of Scientific Instruments **83**, 10D310 (2012).

[10] D. A. Callahan, N. B. Meezan, S. H. Glenzer, A. J. MacKinnon, L. R. Benedetti, D. K. Bradley, J. R. Celeste, P. M. Celliers, S. N. Dixit, T. Doppner, E. G. Dzentitis, S. Glenn, S. W. Haan, C. A. Haynam, D. G. Hicks, D. E. Hinkel, O. S. Jones, O. L. Landen, R. A. London, A. G. MacPhee, P. A. Michel, J. D. Moody, J. E. Ralph, H. F. Robey, M. D. Rosen, M. B. Schneider, D. J. Strozzi, L. J. Suter, R. P. J. Town, K. Widmann, E. A. Williams, M. J. Edwards, B. J. MacGowan, J. D. Lindl, L. J. Atherton, G. A. Kyrala, J. L. Kline, R. E. Olson, D. Edgell, S. P. Regan, A. Nikroo, H. Wilkins, J. D. Kilkenny, and A. S. Moore, Physics of Plasmas **19**, 056305 (2012).

[11] M. Rosen, H. Scott, D. Hinkel, E. Williams, D. Callahan, R. Town, L. Divol, P. Michel, W. Kruer, L. Suter, R. London, J. Harte, and G. Zimmerman, High Energy Density Physics **7**, 180 (2011).

[12] R. P. J. Town, M. D. Rosen, P. A. Michel, L. Divol, J. D. Moody, G. A. Kyrala, M. B. Schneider, J. L. Kline, C. A. Thomas, J. L. Milovich, D. A. Callahan, N. B. Meezan, D. E. Hinkel, E. A. Williams, R. L. Berger, M. J. Edwards, L. J. Suter, S. W. Haan, J. D. Lindl, E. L. Dewald, S. Dixit, S. H. Glenzer, O. L. Landen, E. I. Moses, H. A. Scott, J. A. Harte, and G. B. Zimmerman, Physics of Plasmas **18**, 056302 (2011).

[13] P. Michel, L. Divol, E. Williams, S. Weber, C. Thomas, D. Callahan, S. Haan, J. Salmonson, S. Dixit, D. Hinkel, M. Edwards, B. MacGowan, J. Lindl, S. Glenzer, and L. Suter, Physical Review Letters **102**, 025004 (4 pp.) (2009).

[14] P. Michel, S. H. Glenzer, L. Divol, D. K. Bradley, D. Callahan, S. Dixit, S. Glenn, D. Hinkel, R. K. Kirkwood, J. L. Kline, W. L. Kruer, G. A. Kyrala, S. L. Pape, N. B. Meezan, R. Town, K. Widmann, E. A. Williams, B. J. MacGowan, J. Lindl, and L. J. Suter, Physics of Plasmas **17**, 056305 (2010).

[15] O. S. Jones, C. J. Cerjan, M. M. Marinak, J. L. Milovich, H. F. Robey, P. T. Springer, L. R. Benedetti, D. L. Bleuel, E. J. Bond, D. K. Bradley, D. A. Callahan, J. A. Caggiano, P. M. Celliers, D. S. Clark, S. M. Dixit, T. Doppner, R. J. Dylla-Spears, E. G. Dzentitis, D. R. Farley, S. M. Glenn, S. H. Glenzer, S. W. Haan, B. J. Haid, C. A. Haynam, D. G. Hicks, B. J. Kozioziemski, K. N. LaFortune, O. L. Landen, E. R. Mapoles, A. J. MacKinnon, J. M. McNaney, N. B. Meezan, P. A. Michel, J. D. Moody, M. J. Moran, D. H. Munro, M. V. Patel, T. G. Parham, J. D. Sater, S. M. Sepke, B. K. Spears, R. P. J. Town, S. V. Weber, K. Widmann, C. C. Widmayer, E. A. Williams, L. J. Atherton, M. J. Edwards, J. D. Lindl, B. J. MacGowan, L. J. Suter, R. E. Olson, H. W. Herrmann, J. L. Kline, G. A. Kyrala, D. C. Wilson, J. Frenje, T. R. Boehly, V. Glebov, J. P. Knauer, A. Nikroo, H. Wilkens, and J. D. Kilkenny, Physics of Plasmas **19**, 056315 (2012).

[16] D. S. Clark, D. E. Hinkel, D. C. Eder, O. S. Jones, S. W. Haan, B. A. Hammel, M. M. Marinak, J. L. Milovich, H. F. Robey, L. J. Suter, and R. P. J. Town, "Detailed implosion modeling of deuterium-tritium layered experiments on the National Ignition Facility," submitted to Phys. Plasmas.

[17] J. L. Kline, D. A. Callahan, S. H. Glenzer, N. B. Meezan, J. D. Moody, O. S. Jones, A. J. MacKinnon, R. Bennedetti, R. L. Berger, D. K. Bradley, E. L. Dewald, I. Bass, C. Bennett, M. Bowers, G. Brunton, J. Bude, S. Burkhart, A. Condor, J. M. D. Nicola, P. D. Nicola, S. N. Dixit, T. Döppner, E. G. Dzenitis, G. Erbert, J. Folta, G. Grim, S. Glenn, A. Hamza, S. W. Haan, J. Heebner, M. Henesian, M. Hermann, D. G. Hicks, D. E. Hinkel, W. W. Hsing, K. Jancaitis, O. S. Jones, D. Kalantar, S. F. Khan, G. A. Kyrala, K. LaFortune, O. L. Landen, L. Lagin, D. Larson, T. Ma, A. G. MacPhee, P. A. Michel, P. Miller, M. Montincelli, A. S. Moore, A. Nikroo, M. Mostrand, R. E. Olson, A. Pak, J. P. Patel, L. Pelz, J. Ralph, S. P. Regan, H. F. Robey, M. D. Rosen, S. Ross, M. B. Schneider, M. Shaw, D. J. Strozzi, T. Suratwala, L. J. Suter, R. P. J. Town, B. V. Wonterghem, P. Wegner, K. Widmann, C. Widmayer, H. Wilkens, E. A. Williams, M. J. Edwards, B. J. MacGowan, J. D. Kilkenn, J. D. Lindl, L. J. Atherton, and E. I. Moses, "Hohlraum energetics scaling to 520 TW on the

National Ignition Facility," submitted to Phys. Plasmas.

[18] N. B. Meezan, D. G. Hicks, D. A. Callahan, R. E. Olson, M. S. Schneider, C. A. Thomas, H. F. Robey, P. M. Celliers, J. L. Kline, S. N. Dixit, P. A. Michel, O. S. Jones, D. S. Clark, J. E. Ralph, T. Döppner, A. J. MacKinnon, S. W. Haan, O. L. Landen, S. H. Glenzer, L. J. Suter, M. J. Edwards, B. J. MacGowan, J. D. Lindl, and L. J. Atherton, "Hohlraum designs for high velocity implosions on NIF," To be published in the Proceedings of the Seventh International Conference on Inertial Fusion Sciences and Applications, EPJ Web of Conferences.

[19] E. L. Dewald, K. M. Campbell, R. E. Turner, J. P. Holder, O. L. Landen, S. H. Glenzer, R. L. Kauffman, L. J. Suter, M. Landon, M. Rhodes, and D. Lee, Review of Scientific Instruments **75**, 3759 (2004).

[20] J. L. Kline, K. Widmann, A. Warrick, R. E. Olson, C. A. Thomas, A. S. Moore, L. J. Suter, O. Landen, D. Callahan, S. Azevedo, J. Liebman, S. H. Glenzer, A. Conder, S. N. Dixit, P. Torres, III, V. Tran, E. L. Dewald, J. Kamperschroer, L. J. Atherton, J. R. Beeler, L. Berzins, J. Celeste, C. Haynam, W. Hsing, D. Larson, B. J. MacGowan, D. Hinkel, D. Kalantar, R. Kauffman, J. Kilkenny, N. Meezan, M. D. Rosen, M. Schneider, E. A. Williams, S. Vernon, R. J. Wallace, B. V. Wonterghem, and B. K. Young, Review of Scientific Instruments **81**, 10E321 (2010).

[21] M. B. Schneider, O. S. Jones, N. B. Meezan, J. L. Milovich, R. P. Town, S. S. Alvarez, R. G. Beeler, D. K. Bradley, J. R. Celeste, S. N. Dixit, M. J. Edwards, M. J. Haugh, D. H. Kalantar, J. L. Kline, G. A. Kyrala, O. L. Landen, B. J. MacGowan, P. Michel, J. D. Moody, S. K. Oberhelman, K. W. Piston, M. J. Pivovaroff, L. J. Suter, A. T. Teruya, C. A. Thomas, S. P. Vernon, A. L. Warrick, K. Widmann, R. D. Wood, and B. K. Young, Review of Scientific Instruments **81**, 10E538 (2010).